

# Parametric control of a superconducting flux qubit

S. Saito,<sup>1,2</sup> T. Meno,<sup>3</sup> M. Ueda,<sup>1,2,4</sup> H. Tanaka,<sup>1,2</sup> K. Semba,<sup>1,2</sup> and H. Takayanagi<sup>1,2</sup>

<sup>1</sup>*NTT Basic Research Laboratories, NTT Corporation, Atsugi, Kanagawa 243-0198, Japan*

<sup>2</sup>*CREST, Japan Science and Technology Agency, Kawaguchi, Saitama 332-0012, Japan*

<sup>3</sup>*NTT Advanced Technology Corporation, Atsugi, Kanagawa 243-0198, Japan*

<sup>4</sup>*Department of Physics, Tokyo Institute of Technology, Meguro, Tokyo 152-8551, Japan*

Parametric control of a superconducting flux qubit has been achieved by using two-frequency microwave pulses. We have observed Rabi oscillations stemming from parametric transitions between the qubit states when the sum of the two microwave frequencies or the difference between them matches the qubit Larmor frequency. We have also observed multi-photon Rabi oscillations corresponding to one- to four-photon resonances by applying single-frequency microwave pulses. The parametric control demonstrated in this work widens the frequency range of microwaves for controlling the qubit and offers a high quality testing ground for exploring nonlinear quantum phenomena.

PACS numbers: 74.50.+r, 03.67.Lx, 42.50.Hz, 85.25.Dq

Quantum state engineering has become one of the most important arenas in quantum physics. In particular, the coherent control of quantum two-state systems (TSS), which are applicable to quantum bits (qubit), has attracted increasing interest in the context of quantum computing and quantum information processing [1]. Various candidate physical systems are being studied for the future implementation of qubits. These include artificial quantum TSS like superconducting qubits [2, 3, 4, 5, 6, 7, 8, 9] as well as naturally existing quantum TSS like nuclear spins [10, 11]. Of the many candidates that may enable us to realize quantum computation, superconducting qubits based on Josephson junctions have gained increasing importance because of their potential controllability and scalability.

The coherent control of a single qubit has been demonstrated in many types of superconducting circuits, such as charge [2], charge-phase [3], phase [4, 5], and flux qubits [7, 8, 9]. Recently, two-qubit operation has been demonstrated in charge [12] and phase qubits [13]. In addition to qubit operation, the superconducting qubit offers a testing ground for exploring interactions between photons and artificial macroscopic objects, which we shall refer to as “atoms”. In the weak-driving limit, the interaction between a single “atom” and a single microwave photon has been demonstrated with a charge qubit, which is strongly coupled to a superconducting transmission line resonator [14]. In the strong-driving regime, superconducting qubits have exhibited nonlinear optical responses: multi-photon Rabi oscillations have been observed in a charge qubit by using microwave pulses [15], and under continuous microwave irradiation, multi-photon absorption has been observed in a phase [16] and a flux qubit [17].

In this Letter, we describe the parametric control of a superconducting flux qubit with two-frequency microwave pulses. We have succeeded in observing two-photon Rabi oscillations of the qubit caused by a parametric transition when the qubit Larmor frequency

matches either the sum of the two microwave frequencies or the difference between them. We also show multi-photon Rabi oscillations corresponding to one- to four-photon resonances under single-frequency microwave pulse irradiation where the qubit Larmor frequency was equal to multiples of the microwave frequency. The parametric and multi-photon transitions clearly exhibit high nonlinearity due to interactions between a single “atom” and microwaves. In addition, they can be useful when designing practical gate operation on superconducting qubits. For example, two-photon processes can be used to entangle two qubits as already shown in the field of ion trap qubits [18]. Thus, nonlinear effects will offer new possibilities for flexible qubit control as well as being of fundamental physical interest in the field of superconducting qubits.

If we are to observe highly nonlinear phenomena in superconducting qubits with strong microwave driving, the electromagnetic environment of the qubits must be well controlled because the strong driving easily excites unwanted environmental resonances, which destroy the qubit coherence. Our device was fabricated using electron beam lithography and shadow evaporation techniques defining an inner aluminum loop forming the qubit and an outer loop enclosing the dc-SQUID loop used for the readout (Fig. 1(a)). The inner loop contains three Josephson junctions, one with an area  $\alpha \simeq 0.8$  times smaller than the nominally identical area of the other two with critical current  $I_c \approx 430$  nA. The outer loop comprises two Josephson junctions of critical current  $\approx 140$  nA. We placed an on-chip microwave line close to the qubit at a distance of  $20 \mu\text{m}$  so that the qubit could be strongly driven by oscillating magnetic fields, which are induced by microwave currents flowing through the line. To control the electromagnetic environment surrounding the qubit, we put resistors  $R_{I1}$ ,  $R_{V1}$ , lead inductances  $L$ , and shunt capacitors  $C$ ,  $2C$  on the chip (Fig. 1(b)). The resistors damp unwanted resonances, which are generated in, for example, leads and parasitic capacitors outside the

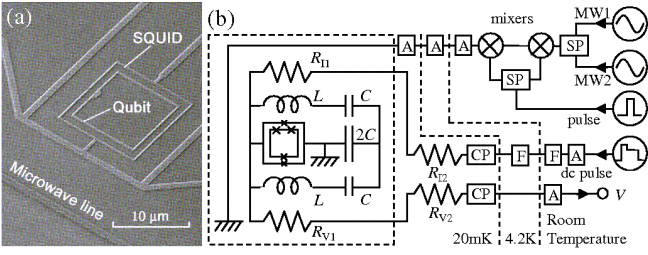


FIG. 1: (a) Scanning electron micrograph of a flux qubit (inner loop) and a dc-SQUID (outer loop). The loop sizes of the qubit and SQUID are  $10.2 \times 10.4 \mu\text{m}^2$  and  $12.6 \times 13.5 \mu\text{m}^2$ , respectively. They are magnetically coupled by the mutual inductance  $M \approx 13 \text{ pH}$ . (b) A circuit diagram of the flux qubit measurement system. On-chip components are shown in the dashed box. Surface mount resistors  $R_{11} = 0.9 \text{ k}\Omega$ ,  $R_{V1} = 5 \text{ k}\Omega$  and  $R_{V2} = 3 \text{ k}\Omega$  are set in the sample holder. We put adequate copper powder filters CP and LC filters F and attenuators A for each line.

resistors. There are two well-controlled resonance modes that are produced in the circuits inside the resistors, namely, the on-chip components close to the qubit. One is the dc-SQUID's plasma mode with a frequency of 1.0 GHz, which is formed in the two symmetrical loops, each being composed of  $L$ ,  $C$ ,  $2C$ , and the SQUID's Josephson inductance. The other is the harmonic LC resonance mode with a frequency of 4.311 GHz, which is produced in the larger loop consisting of the two  $L$ 's and the two  $C$ 's. In this way, we have achieved an artificial TSS in a well-controlled environment.

The three Josephson junctions of the qubit form a double-well potential in the space of the Josephson phase when about half a flux quantum threads the qubit loop. We use the two lowest levels in the potential as the qubit states, which are well separated from the higher levels. Thus, the qubit is described by the Hamiltonian  $H_{\text{qb}} = (\hbar/2)(\varepsilon\sigma_z + \Delta\sigma_x)$ , where  $\sigma_{x,z}$  are the Pauli spin matrices. The eigenstates of  $\sigma_z$  describe clockwise and counter-clockwise persistent currents in the qubit. The qubit tunnel splitting is described by  $\hbar\Delta$ , and  $\hbar\varepsilon = 2I_p\Phi_0(\Phi_{\text{qb}}/\Phi_0 - 1.5)$  is the energy imbalance between the two potential wells caused by the externally applied magnetic flux threading the qubit loop  $\Phi_{\text{qb}}$ , where  $\Phi_0 = h/2e$  is the flux quantum and  $I_p = I_c\sqrt{1 - (1/2\alpha)^2}$  is the magnitude of the qubit persistent current when the qubit is in the  $\sigma_z$  eigenstates and  $I_c$  is the critical current of the larger junctions. The energy difference between the ground state  $|g\rangle$  and the first excited state  $|e\rangle$  of the qubit is  $\hbar\omega_{\text{qb}} = \hbar f_{\text{qb}} = \hbar\sqrt{\varepsilon^2 + \Delta^2}$ . Assuming that the applied microwaves are in coherent states, we may describe the qubit under microwave irradiation by the Hamiltonian

$$H = \frac{\hbar}{2} (\varepsilon\sigma_z + \Delta\sigma_x) + \sum_{k=1}^l 2\hbar g_k \alpha_k \sigma_z \cos \omega_{\text{MW}k} t, \quad (1)$$

where  $l$  is one (two) in the case of a single- (two-) frequency microwave and  $g_k$  is the coupling between the qubit and the  $k$ -th microwave (MW $k$ ), whose amplitude and frequency are  $\alpha_k$  and  $f_{\text{MW}k} = \omega_{\text{MW}k}/2\pi$ , respectively. Solving the Schrödinger equation with the Hamiltonian (1) without the rotating wave approximation, we obtain the time evolution of the probability  $P_e(t)$  with which we find the qubit in  $|e\rangle$ . The probability  $P_e(t)$  oscillates periodically under resonant conditions  $\omega_{\text{qb}} = n_1\omega_{\text{MW}1}$  (for the single-frequency microwave) or  $\omega_{\text{qb}} = |n_1\omega_{\text{MW}1} \pm n_2\omega_{\text{MW}2}|$  (for the two-frequency microwave), where  $n_k$  is the MW $k$  photon number. When we operate the qubit away from its degeneracy point  $\varepsilon \neq 0$ , the frequency of the oscillation is given for the single-frequency microwave irradiation by

$$\Omega_{\text{Rabi}} = \frac{\Delta}{A} J_{n_1} \left( A \frac{4g_1\alpha_1}{\omega_{\text{MW}1}} \right) \quad (2)$$

and for the two-frequency microwave irradiation by

$$\Omega_{\text{Rabi}} = \frac{\Delta}{A} J_{n_1} \left( A \frac{4g_1\alpha_1}{\omega_{\text{MW}1}} \right) J_{n_2} \left( A \frac{4g_2\alpha_2}{\omega_{\text{MW}2}} \right). \quad (3)$$

Here  $J_{n_k}$  is the  $n_k$ -th order Bessel function of the first kind and  $A \equiv \varepsilon/\omega_{\text{qb}} \approx 1$ . This approximation is valid when  $\varepsilon \gg \Delta$ . The dressed atom approach gives results similar to Eq. (2) [15, 19].

The measurements were carried out in a dilution refrigerator. The sample was mounted in a gold plated copper box that was thermalized to the base temperature of 20 mK ( $k_B T \ll \hbar\omega_{\text{qb}}$ ). To produce two-frequency microwave pulses, we added two microwaves MW1 and MW2 with frequencies of  $f_{\text{MW}1}$  and  $f_{\text{MW}2}$ , respectively by using a splitter SP (Fig. 1(b)). Then we shaped them into microwave pulses through two mixers. We measured the amplitude of MW $k$   $V_{\text{MW}k}$  at the point between the attenuator and the mixer with an oscilloscope. We confirmed that unwanted higher-order frequency components in the pulses, for example  $|f_{\text{MW}1} \pm f_{\text{MW}2}|$ ,  $2f_{\text{MW}1}$ , and  $2f_{\text{MW}2}$  are negligibly small under our experimental conditions. First, we choose the operating point by setting  $\Phi_{\text{qb}}$  around  $1.5\Phi_0$ , which fixes the qubit Larmor frequency  $f_{\text{qb}}$ . The qubit is thermally initialized to be in  $|g\rangle$  by waiting for 300  $\mu\text{s}$ , which is much longer than the qubit energy relaxation time (for example 3.8  $\mu\text{s}$  at  $f_{\text{qb}} = 11.1 \text{ GHz}$ ). Then a qubit operation is performed by applying a microwave pulse to the qubit. The pulse, with an appropriate length  $t_p$ , amplitudes  $V_{\text{MW}k}$ , and frequencies  $f_{\text{MW}k}$ , prepares a qubit in the superposition state of  $|g\rangle$  and  $|e\rangle$ . After the operation, we immediately apply a dc readout pulse to the dc-SQUID. This dc pulse consists of a short (70 ns) initial pulse followed by a long (1.5  $\mu\text{s}$ ) trailing plateau that has 0.6 times the amplitude of the initial part. For  $\Phi_{\text{qb}} < 1.5\Phi_0$ , if the qubit is detected as being in  $|e\rangle$ , the SQUID switches to a voltage state and an output voltage pulse should be observed;

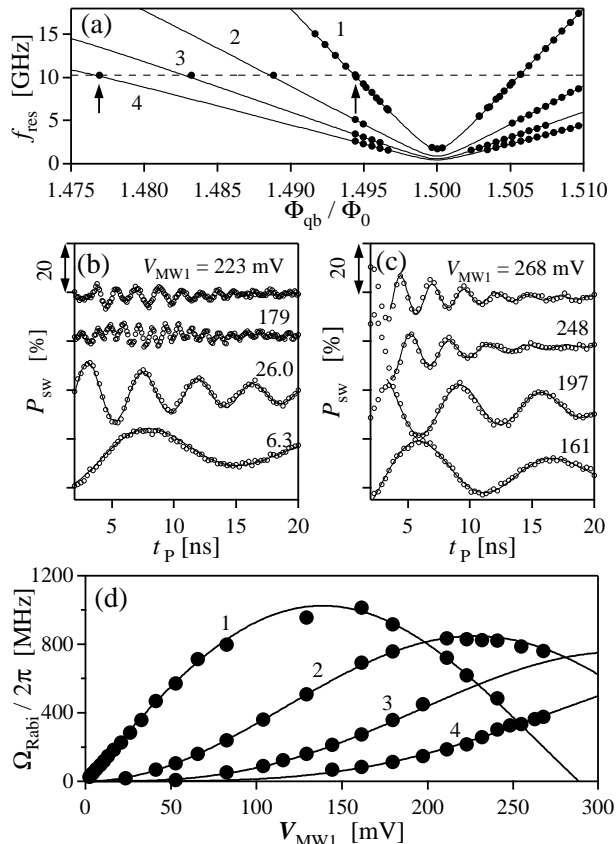


FIG. 2: Experimental results with single-frequency microwave pulses. (a) Spectroscopic data of the qubit. Each set of the dots represents the resonant frequencies  $f_{\text{res}}$  caused by the one to four-photon absorption processes. The solid curves are numerical fits. The dashed line shows a microwave frequency  $f_{\text{MW1}}$  of 10.25 GHz. (b) One-photon Rabi oscillations of  $P_{\text{sw}}$  with exponentially damped oscillation fits. Both the qubit Larmor frequency  $f_{\text{qb}}$  and the microwave frequency  $f_{\text{MW1}}$  are 10.25 GHz. The external flux is  $\Phi_{\text{qb}}/\Phi_0 = 1.4944$ . (c) Four-photon Rabi oscillations when  $f_{\text{qb}} = 41.0$  GHz,  $f_{\text{MW1}} = 10.25$  GHz, and  $\Phi_{\text{qb}}/\Phi_0 = 1.4769$ . (d) The microwave amplitude dependence of the Rabi frequencies  $\Omega_{\text{Rabi}}/2\pi$  up to four-photon Rabi oscillations. The solid curves represent theoretical fits.

otherwise there should be no output voltage pulse. By repeating the measurement 8000 times, we obtain the SQUID switching probability  $P_{\text{sw}}$ , which is directly related to  $P_e(t_p)$  for the dc readout pulse with a proper amplitude. For  $\Phi_{\text{qb}} > 1.5\Phi_0$ ,  $P_{\text{sw}}$  is directly related to  $1 - P_e(t_p)$ .

We performed a spectroscopy measurement of the qubit with long (50 ns) single-frequency microwave pulses. We observed multi-photon resonant peaks ( $\Phi_{\text{qb}} < 1.5\Phi_0$ ) and dips ( $\Phi_{\text{qb}} > 1.5\Phi_0$ ) in the dependence of  $P_{\text{sw}}$  on  $f_{\text{MW1}}$  at a fixed magnetic flux  $\Phi_{\text{qb}}$ . We obtained the qubit energy diagram by plotting their positions as

a function of  $\Phi_{\text{qb}}/\Phi_0$  (Fig. 2(a)). We took the data around the degeneracy point  $\Phi_{\text{qb}} \approx 1.5\Phi_0$  by applying an additional dc pulse to the microwave line to shift  $\Phi_{\text{qb}}$  away from  $1.5\Phi_0$  just before the readout, because the dc-SQUID could not distinguish the qubit states around the degeneracy point. The top solid curve in Fig. 2(a) represents a numerical fit to the resonant frequencies of one-photon absorption. From this fit, we obtain the qubit parameters  $E_J/h = 213$  GHz,  $\Delta/2\pi = 1.73$  GHz, and  $\alpha = 0.8$ . The other curves in Fig. 2(a) are drawn by using these parameters for  $n_1 = 2, 3$ , and 4.

Next, we used short single-frequency microwave pulses with a frequency of 10.25 GHz to observe the coherent quantum dynamics of the qubit. Figures 2(b) and (c) show one- and four-photon Rabi oscillations observed at the operating points indicated by arrows in Fig. 2(a) with various microwave amplitudes  $V_{\text{MW1}}$ . These data can be fitted by damped oscillations  $\propto \exp(-t_p/T_d) \cos(\Omega_{\text{Rabi}}t_p)$ , except for the upper two curves in Fig. 2(b). Here,  $t_p$  and  $T_d$  are the microwave pulse length and qubit decay time, respectively. To obtain  $\Omega_{\text{Rabi}}$ , we performed a fast Fourier transform (FFT) on the curves that we could not fit by damped oscillations. Although we controlled the qubit environment, there were some unexpected resonators coupled to the qubit, which could be excited by the strong microwave driving or by the Rabi oscillations of the qubit. We consider that these resonators degraded the Rabi oscillations in the higher  $V_{\text{MW1}}$  range of Fig. 2(b). Figure 2(d) shows the  $V_{\text{MW1}}$  dependences of  $\Omega_{\text{Rabi}}/2\pi$  up to four-photon Rabi oscillations, which are well reproduced by Eq. (2). Here, we used only one scaling parameter  $a(10.25 \text{ GHz}) = 0.013$  defined as  $a(f_{\text{MW1}}) \equiv 4g_1\alpha_1/\omega_{\text{MW1}}V_{\text{MW1}}$ , because it is hard to measure the real amplitude of the microwave applied to the qubit at the sample position. The scaling parameter  $a(f_{\text{MW1}})$  reflects the way in which the applied microwave is attenuated during its transmission to the qubit and the efficiency of the coupling between the qubit and the on-chip microwave line. In this way, we can estimate the real microwave amplitude and the interaction energy between the qubit and the microwave  $2\hbar g_1\alpha_1$  by fitting the dependence of  $\Omega_{\text{Rabi}}/2\pi$  on  $V_{\text{MW1}}$ . These results show that we can reach a driving regime that is so strong that the interaction energy  $2\hbar g_1\alpha_1$  is larger than the qubit transition energy  $\hbar\omega_{\text{qb}}$ .

We have also performed experiments with two microwave frequencies  $f_{\text{MW1}}$  and  $f_{\text{MW2}}$ . First, we carried out a spectroscopy measurement by using long (50 ns) two-frequency microwave pulses. In addition to resonances caused by the multi-photon absorption processes at multiples of each microwave frequency ( $f_{\text{qb}} = n_1f_{\text{MW1}}, n_2f_{\text{MW2}}$ ), we also clearly observed those due to parametric processes ( $f_{\text{qb}} = |f_{\text{MW1}} \pm f_{\text{MW2}}|$ ) (not shown).

We next investigated the coherent oscillations of the qubit through the parametric processes by using short two-frequency microwave pulses. Figure 3(a) [(b)] shows

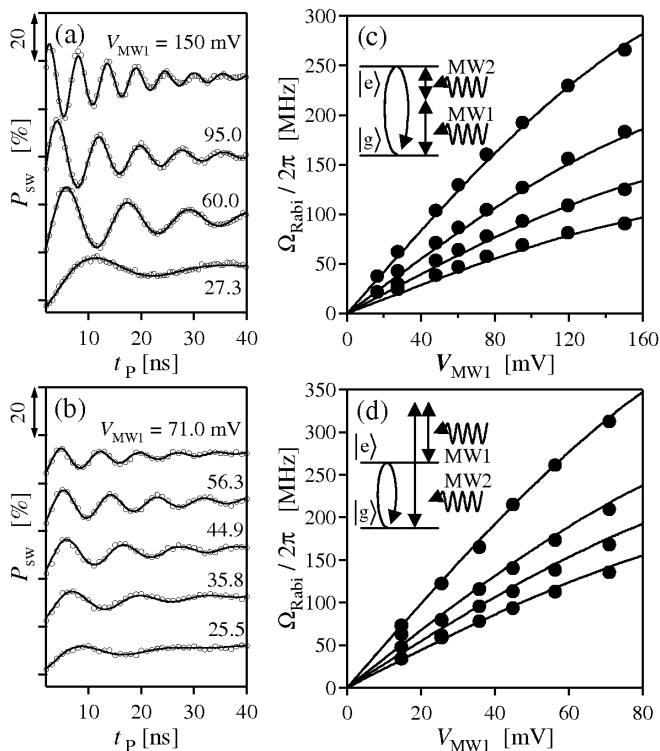


FIG. 3: Experimental results with two-frequency microwave pulses. (a) [(b)] Two-photon Rabi oscillations due to a parametric process when  $f_{\text{qb}} = f_{\text{MW2}} + [-] f_{\text{MW1}}$ . The solid curves are fits by exponentially damped oscillations. (c) [(d)] Rabi frequencies as a function of  $V_{\text{MW1}}$ , which are obtained from the data in Fig. 3(a) [(b)]. The dots represent experimental data when  $V_{\text{MW2}} = 16.9, 23.5, 33.0,$  and  $52.0$  [50.1, 62.9, 79.1, and 124.7] mV from the bottom set of dots to the top one. The solid curves represent Eq. (3). The inset is a schematic of the parametric process that causes two-photon Rabi oscillation when  $f_{\text{qb}} = f_{\text{MW2}} + [-] f_{\text{MW1}}$ .

the Rabi oscillations of  $P_{\text{sw}}$  when the qubit Larmor frequency  $f_{\text{qb}} = 26.45$  [7.4] GHz corresponds to the sum of the two microwave frequencies  $f_{\text{MW1}} = 16.2$  GHz,  $f_{\text{MW2}} = 10.25$  GHz [the difference between  $f_{\text{MW1}} = 11.1$  GHz and  $f_{\text{MW2}} = 18.5$  GHz] and the microwave amplitude of MW2  $V_{\text{MW2}}$  was fixed at 33.0 [50.1] mV. They are well fitted by exponentially damped oscillations  $\propto \exp(-t_p/T_d) \cos(\Omega_{\text{Rabi}} t_p)$ . The Rabi frequencies obtained from the data in Fig. 3(a) [(b)] are well reproduced by Eq. (3) without any fitting parameters (Fig. 3(c) [(d)]). Here, we used  $\Delta$ , which was obtained from the spectroscopy measurement (Fig. 2(a)) and used  $a(10.25 \text{ GHz}) = 0.013$  and  $a(16.2 \text{ GHz}) = 0.0074$  [ $a(11.1 \text{ GHz}) = 0.013$  and  $a(18.5 \text{ GHz}) = 0.0082$ ], which had been obtained from Rabi oscillations by using single-frequency microwave pulses with each frequency. Those results provide strong evidence that we can achieve parametric control of the qubit with two-frequency microwave pulses.

In summary, we investigated nonlinear responses in the

superconducting flux qubit. First, we observed multi-photon Rabi oscillations caused by up to four-photon transitions by using single-frequency microwave pulses. The microwave amplitude dependences of the Rabi frequencies are well reproduced by Bessel functions derived from a semi-classical model. Furthermore, we successfully demonstrated parametric control of the qubit by using two-frequency microwave pulses. We observed Rabi oscillations of the qubit caused by parametric transitions when  $f_{\text{qb}} = |f_{\text{MW1}} \pm f_{\text{MW2}}|$ . The Rabi frequencies as a function of the microwave amplitudes are well described by the product of two Bessel functions. These results indicate that the flux qubit offers a good testing ground for exploring quantum nonlinear phenomena in a macroscopic quantum object. Furthermore, these multi-photon processes observed in our experiment widen the frequency range of microwaves for controlling flux qubit.

We thank T. Kutsuzawa, F. Deppe for useful discussions and for helping with the experimental setup. We also acknowledge useful discussions with J. Johansson, H. Nakano, M. Thorwart, Y. Yamamoto, J. E. Mooij, C. J. P. M. Harmans, and Y. Nakamura. This work has been supported by the CREST project of the Japan Science and Technology Agency (JST).

- 
- [1] M. A. Nielsen and I. L. Chuang, *Quantum Computation and Quantum information* (Cambridge Univ. Press, Cambridge, 2000).
  - [2] Y. Nakamura, Y. A. Pashkin, and J. S. Tsai, *Nature* **398**, 786 (1999).
  - [3] D. Vion *et al.*, *Science* **296**, 886 (2002).
  - [4] Y. Yu, S. Han, X. Chu, S.-I. Chu, and Z. Wang, *Science* **296**, 889 (2002).
  - [5] J. M. Martinis, S. Nam, J. Aumentado, and C. Urbina, *Phys. Rev. Lett.* **89**, 117901 (2002).
  - [6] J. E. Mooij *et al.*, *Science* **285**, 1036 (1999).
  - [7] I. Chiorescu, Y. Nakamura, C. J. P. M. Harmans, and J. E. Mooij, *Science* **299**, 1869 (2003).
  - [8] T. Kutsuzawa *et al.*, *Appl. Phys. Lett.* (to be published); cond-mat/0501592.
  - [9] B. L. T. Ploude *et al.*, cond-mat/0501679.
  - [10] L. M. K. Vandersypen *et al.*, *Nature* **414**, 883 (2001).
  - [11] G. Yusa, K. Muraki, K. Hashimoto, and Y. Hirayama, *Nature* **434**, 1001 (2005).
  - [12] T. Yamamoto, Y. A. Pashkin, O. Astafiev, Y. Nakamura, and J. S. Tsai, *Nature* **425**, 941 (2003).
  - [13] R. McDermott *et al.*, *Science* **307**, 1299 (2005).
  - [14] A. Wallraff *et al.*, *Nature* **431**, 162 (2004).
  - [15] Y. Nakamura, Y. A. Pashkin, and J. S. Tsai, *Phys. Rev. Lett.* **87**, 246601 (2001).
  - [16] A. Wallraff, T. Duty, A. Lukashenko, and A. V. Ustinov, *Phys. Rev. Lett.* **90**, 037003 (2003).
  - [17] S. Saito *et al.*, *Phys. Rev. Lett.* **93**, 037001 (2004).
  - [18] C. A. Sackett *et al.*, *Nature* **404**, 256 (2000).
  - [19] C. Cohen-Tannoudji, J. Dupont-Roc, and G. Grynberg, *Atom-Photon Interactions* (Wiley, New York, 1992).